WOOD RESEARCH
57 (1): 2012
57-68

MECHANICAL BEHAVIOR OF SPRUCE UNDER TRIAXIAL COMPRESSION

József Garab
University of West Hungary, Institute for Applied Mechanics and Structures
Sopron, Hungary

Roland Reihsner, Josef Eberhardsteiner
Vienna University of Technology, Institute for Mechanics of Materials and Structures
Vienna, Austria

(Received May 2011)

ABSTRACT

Inspection of the mechanical behavior of wood under a multiaxial load is a challenging study. The goal of this work was to perform triaxial compression experiments with a servo-hydraulic testing machine with different side pressures on cylindrical specimens of spruce (*Picea abies*) with varying grain angles. The triaxial compression strength and the axial stress-strain relationship were determined. The obtained results show that the influence of the grain angle on the mechanical behavior of spruce wood is similar as in the uniaxial case. The triaxial compression strength and the stiffness parameters decrease with increasing growth ring angles from the longitudinal direction to 45°. The side pressure mainly influences the stiffness, particularly the longitudinal oriented samples. Although the shear effect is remarkable in the cross grained specimens, the role of the side pressure is not completely clear yet; further investigations are necessary.

KEYWORDS: Spruce, orientation, triaxial compression, complex stress state, strength, axial stress-strain relationship.

INTRODUCTION

Wood is a basic structural material; therefore its mechanical properties are often discussed. Among others Kollmann (1951), Niemz (1993) and the Forest Products Laboratory (2000) reported the mechanical properties of common wood species used in the wood industry. In Europe, spruce (*Picea abies*) is the most prevalent wood species. Therefore numerous works focused on the determination of the mechanical properties of spruce wood (e.g. Neuhaus 1981, Szalai 1998, Reiterer and Stanzl-Tschegg 2001, Gindl and Teischinger 2002, Keunecke et al.

2008, Garab et al. 2010). In the experiments of these studies mostly uniaxial loads were applied resulting in simple stress states in the wood sample.

However, wooden constructions are rarely under uniaxial stress states. The joints are particularly dangerous zones (Fleischmann et al. 2007) characterized by biaxial or triaxial stress states. Therefore investigation of the mechanical response of wood under complex stress states is important. Although creating clear multiaxial stress states is a challenging study, the researchers tried to study the mechanical behavior of wood under combined loading. Yamasaki-Sasaki (2003, 2004) investigated the elastic and the yield properties of wood under static axial-torsion combined loads. In addition, Sasaki and Yamasaki (2002, 2004) Sasaki et al. (2005, 2007) applied pulsating axial-torsion combined loads to generate multiaxial stress states and investigated the mechanical response of wood. Furthermore, Eberhardsteiner (2002) carried out static biaxial experiments on spruce wood. He tested more than 400 samples under varying load combinations and grain orientations and the results provided a basis of other studies to investigate the failure properties of wood (e.g. Mackenzie-Helnwein et al. 2005, Seweryn and Romanovich 2007, Garab and Szalai 2010).

A possible experimental extension can be triaxial compression tests to generate multiaxial stress states on wood. Only few publications are available in connection with triaxial compression loading on wood. Saliklis et al. (1998) tested paperboard and wood under multiaxial compression because packaging and container designs are becoming increasingly complicated and triaxial compression tests were also lacking. In that study, a uniaxial load was applied on cubic wood samples within a confined box. Therefore the lateral expansion generated the two other load directions. Those results show that if a cubic specimen is used, local fracture and unknown friction forces arise which influence the mechanical properties.

These side effects can be reduced by using geotechnical fixtures, which are often used for testing concrete (e.g. Bongers and Rutten 1998, Sfer et al. 2002, Elkadi and van Mier 2006). Otherwise, Ashkenazi et al. (1973) tested spherical and cylindrical solid and modified birch samples under hydrostatic pressure and investigated the fracture properties. Testing wood with similar methods can be a good solution to create complex stress states on wood samples.

MATERIAL AND METHODS

Multiaxial compression tests with a servo-hydraulic triaxial testing machine were carried out on spruce wood. The spruce log originated in Hungary. The lumbers were stored for years.

Specimens

Cylindrical specimens from spruce wood were prepared with dimensions of 50 mm (diameter) and 100 mm (length). Specimens with approximately equal growth ring widths were taken from the outer heartwood region. Therefore orthotropic material behavior can be assumed. Samples with defects such as large knots or compression wood were omitted. However, a few samples contained a few small knots (<5 mm). The specimens were not acclimatized. After determining the moisture content by oven drying, the specimens were tested. Density and moisture content of the samples varied from 0.34 to 0.45 $g.cm^{-3}$ and 12.31 to 14.83 %, respectively. Three different orientations were cut from the sample pieces. The grain angles (φ) were measured from the longitudinal axes and were as follows: 0° (longitudinal), 22° and 45°. Due to the rotational symmetry of the cylindrical specimen, the growth ring angle plays (θ) no role. Each side pressure/orientation combination was tested on six samples. Therefore 54 samples were prepared (three different side pressures was applied, as discussed later) for the static tests.

In addition, four longitudinal oriented samples were made for the cyclic tests. Fig. 1 shows the specimen preparation, orientation and the loading directions on the cylindrical sample.

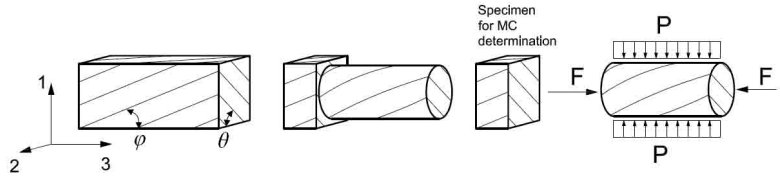

Fig. 1: Specimen preparation, orientation and applied loads. Slats with φ =0° (L), 22° and 45° grain direction and with a cross section of 60 x 60 mm were planed; then the cylindrical part was turned, and finally the prismatic part was cut which was used for the determination of the moisture content. The axial load was applied along the axis 3, while the side pressures along the axis 1 and 2.

Triaxial compression experiments

The cylindrical specimens were tested with a triaxial servo-hydraulic testing machine (Walter und Bai, Typ: DLV-250/DZ-10). The equipment has a 250 kN built-in load cell to measure the axial force. The side pressure was applied using a chamber with 15 MPa hydrostatic pressure. According to Niemz (1993) the transverse uniaxial compression strength is 5.8 MPa and the experiments from Szalai (1998) provided a compression strength of 3.49 MPa in the transverse direction. Thus, the side pressure applied was 0.5, 1.0, and 1.5 MPa to avoid fracture of the samples due to the side pressure only. Axial loading rates of 1 $mm.min^{-1}$ were chosen both for the static and for the cyclic tests.

The testing equipment consists of three main parts: the testing machine (which transmits the axial force into the sample), the triaxial load cell and the specimen holder. First the specimen was placed into a thin rubber hose to avoid lubrication. Then Teflon sheets were placed between wood and the flat steel cylinders to reduce the friction effect. Rubber O-rings were used to fix the flat steel cylinders to the sample. Then, the specimen with mounted tools was fixed in the specimen holder. After that, the specimen holder was placed into the pressure chamber. A small axial load was applied on the force transmitting bar (thus on the sample, too) to avoid having the specimen float during the oil filling. Then, the chamber was filled with oil and was closed. Pressure was exerted and when the final value was achieved, the axial load was applied until failure of the specimen was reached. The axial displacement and axial force were monitored. Failure occurred when the force fell back or the force did not change with increasing axial displacement. After failure, the oil was drained and the specimen was removed. The assembly of the measurement system is shown in Fig. 2.

Triaxial compression strength and the axial stress-strain relationship

Due to the multiaxial compression, complex stress and strain states arose in the wood samples. For simplicity, after failure, the axial component (σ^{33}) of the triaxial compression strength was determined as the maximum force from the load cell divided by the cross sectional area of the specimen. The horizontal strength components (σ^{11}, σ^{22}) were equal to the side pressure p (Eq.1):

$$\sigma^{11} = \sigma^{22} = p \qquad \sigma^{33} = F_{max.} A^{-1} \tag{1}$$

where: A denotes the cross-section of the specimen perpendicular to the loading axis. Since the samples were not acclimatized, the axial components of the compression strengths were

calculated at 12 % moisture content using following equation (Kollmann 1951):

$$\sigma_{12} = \sigma_u \frac{20}{32 - u} \tag{2}$$

where: σ_{12} is the axial component of the triaxial compression strength at 12 % moisture content
u is the moisture content
σ_u is the axial component of the triaxial compression strength at moisture content u.

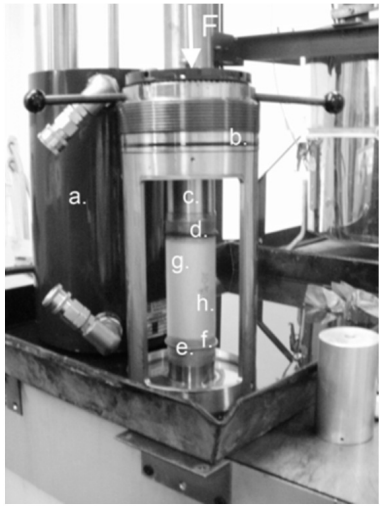

Fig. 2: Testing equipment and the axial load: a) triaxial load cell b) steel fixture c) steel bar d) flat steel cylinder e) rubber O-ring f) Teflon sheet g) cylindrical spruce sample h) rubber hose. The narrow shows the direction of the axial load.

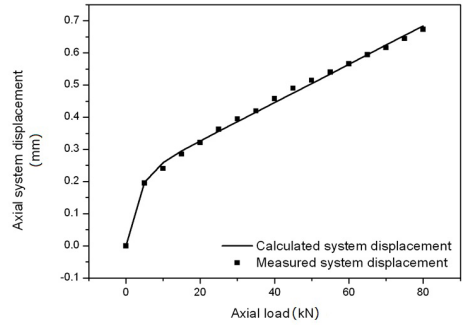

Fig. 3: Calibration of the axial (vertical) system displacement. Exponential fit functioned well on the measurement points.

Thus, the obtained axial stress-strain relationships can be compared to each other.

Unfortunately, no strain gauges could be placed on the wood surfaces due to the closed and pressurized chamber. Although, the strain gauge rosettes can function in the pressurized oil, the cables would have needed space to lead away the signals from the load cell. The small gap between the load transmission steel bar and the insulator ring would have resulted then in oil leaking out and the side pressure on the samples would not be constant. Optical strain measurement could not be done because load cell was not transparent. The strain in the cross directions were also not monitored for the same reason.

However, the axial strain was derived from displacement values, measured by linear variable differential transformers (LVDT). It was assumed that the axial displacement is a function of the axial force. We hypothesized that the testing machine measures the axial displacement from the LVDT and these values contain the axial displacement of the sample and the testing system :

$$\Delta l_{LVDT}(F) = \Delta l_{system}(F) + \Delta l_{sample}(F) \tag{3}$$

If the axial displacement of the sample is determined, the axial displacement of the testing

system may be calculated. Based on this idea, a steel sample with a similar geometric shape to the wood sample was uniaxially tested to calibrate the strain values from the LVDT. The strain was monitored on the steel sample with strain gauge rosettes. The loading rate and the maximum load (80 kN) were the same as for the wood testing. For simplicity, it was assumed that the material of the tested specimen plays no significant role in the axial displacement of the testing system. Thus, the same axial displacement values were assumed in a given force. The system displacement is as follows:

$$\Delta l_{system}(F) = \Delta l_{LVDT}(F) - \Delta l_{steel}(F) \tag{4}$$

$$\Delta l_{system}(F) = \Delta l_{LVDT}(F) - l_{steel}(F) \cdot \varepsilon_{axial}(F) \tag{5}$$

where: ε_{axial} was obtained from the strain gauge glued on the steel sample.

As Fig. 3 shows, an exponential fit functioned well on the measured axial system displacement.

Because of its exponential character, the system displacement was approximated by a function of the axial load as follows:

$$\Delta l_{system}(F) = a + b\left(1 - e^{-cF}\right) \tag{6}$$

The calculated parameters from the exponential fitting were as follows: a=0.0059, b=0.21 and c=0.33. As a result, system displacement was obtained as a function of the force. Thus the axial displacement of the wood samples could be determined indirectly for all axial forces with Eq. (7) as

$$\Delta l_{wood}(F) = \Delta l_{LVDT}(F) - \Delta l_{system}(F) \tag{7}$$

The next step was to determine the axial strain. From the theory of small deformations, Eq. (8) is obvious:

$$\varepsilon_{axial} = \frac{\Delta l_{wood}}{l_0} \tag{8}$$

Thus, the axial stress-strain diagram for each tested specimen could be determined. Its character, the slope of the linear elastic region and the maximum stress value (axial component of the triaxial compression strength) were investigated. The influence of the side pressure and the grain angle were in the focus of the evaluation.

RESULTS AND DISCUSSION

54 specimens were tested with the servo-hydraulic triaxial testing machine. In addition, the axial stress and the axial strain components were determined. In a few samples, high axial stresses arose at the beginning of the tests when maximum side pressure was exerted. This phenomenon occurred in cross-grained samples and they broke only due to the side pressure. The pressurized oil resulted in fractures. Thus, the side pressure influenced the axial stress. Some samples broke due to the side pressure only: one with a 45° grain angle at 0.5 MPa side pressure, two at a 1.0 MPa side pressure, and one at a 1.5 MPa side pressure. Therefore, these tests could not be evaluated.

The failure was not visible in longitudinal oriented samples but cracks occurred parallel to the grain direction in cross grained specimens (Fig. 4). In addition, the specimens were deformed. It agrees with an earlier study. Ashkenazi et al. (1973) reported visible changes in the shape of the specimen if the axis of the cylinder did not coincide with the axis of symmetry of the material.

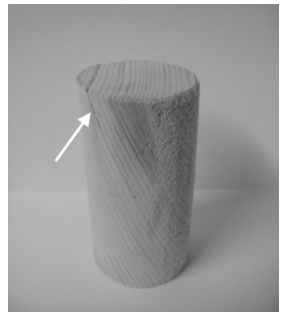

Fig. 4: Cross grained sample (22°) after triaxial compression. Crack arose in the earlywood zone parallel to the grain direction (see arrow). The colorization is due the remove of the oiled rubber shell.

Triaxial compression strength and the axial stress-strain relationship

Tabs. 1-3 contain the results of the experimentally determined triaxial compression strength for each sample.

Tab. l: The components of the triaxial compression strength in case of 0° (longitudinal) grain angle and 0.5, 1.0 and 1.5 MPa side pressure.

Density ($g.cm^{-3}$)	Moisture content (%)	σ^{11} (MPa)	σ^{22} (MPa)	σ^{33} (MPa)
0.36	13.47	0.50	0.50	26.45
0.39	14.34	0.50	0.50	33.45
0.34	14.25	0.50	0.50	30.45
0.36	14.19	0.50	0.50	30.94
0.36	14.24	0.50	0.50	31.47
0.36	14.13	0.50	0.50	30.55
0.41	14.59	1.00	1.00	35.02
0.39	14.24	1.00	1.00	36.52
0.40	14.43	1.00	1.00	32.84
0.39	14.08	1.00	1.00	35.89
0.38	12.57	1.00	1.00	23.51
0.38	14.20	1.00	1.00	34.14
0.37	14.20	1.50	1.50	34.19
0.43	14.83	1.50	1.50	37.92
0.42	14.13	1.50	1.50	39.65
0.36	14.26	1.50	1.50	31.50
0.38	14.36	1.50	1.50	33.72
0.35	14.27	1.50	1.50	31.42

Tab. 2: The components of the triaxial compression strength in case of 22° grain angle and 0.5, 1.0 and 1.5 MPa side pressure.

Density ($g.cm^{-3}$)	Moisture content (%)	σ^{11} (MPa)	σ^{22} (MPa)	σ^{33} (MPa)
0.38	13.75	0.50	0.50	21.94
0.42	13.95	0.50	0.50	17.92
0.41	13.87	0.50	0.50	18.04
0.36	13.95	0.50	0.50	18.49
0.36	14.05	0.50	0.50	18.42
0.38	13.82	0.50	0.50	20.23
0.44	13.64	1.00	1.00	19.27
0.38	13.80	1.00	1.00	17.93
0.39	13.82	1.00	1.00	19.99
0.36	14.25	1.00	1.00	18.52
0.37	14.21	1.00	1.00	17.09
0.37	14.26	1.00	1.00	15.49
0.41	13.86	1.50	1.50	20.77
0.40	13.92	1.50	1.50	16.99
0.45	13.72	1.50	1.50	19.97
0.34	14.21	1.50	1.50	13.62
0.37	14.26	1.50	1.50	11.51
0.36	13.95	1.50	1.50	17.59

Tab. 3: The components of the triaxial compression strength in case of 45° grain angle and 0.5, 1.0 and 1.5 MPa side pressure.

Density ($g.cm^{-3}$)	Moisture content (%)	σ^{11} (MPa)	σ^{22} (MPa)	σ^{33} (MPa)
0.41	13.70	0.50	0.50	9.01
0.45	13.60	0.50	0.50	7.26
0.41	13.69	0.50	0.50	8.61
0.35	13.78	0.50	0.50	8.26
0.36	14.23	0.50	0.50	8.43
0.44	13.57	1.00	1.00	6.45
0.44	13.67	1.00	1.00	6.74
0.42	13.32	1.00	1.00	7.34
0.35	14.20	1.00	1.00	6.71
0.45	13.76	1.50	1.50	6.57
0.43	13.66	1.50	1.50	7.63
0.39	13.76	1.50	1.50	6.33
0.43	13.57	1.50	1.50	6.57
0.43	14.05	1.50	1.50	5.33

Tab. 4 demonstrates the mean values of the axial components of the triaxial compression strength. The values were calculated at 12 % moisture content (MC) by means of Eq. (2) to enable a comparison. Fig. 5 represents the average deviation of the axial stress-strain relationship for a test series with the given grain angles and side pressures.

Tab. 4: The axial components of the triaxial compression strength at 12 % MC in each case of side pressure-orientation combination: mean values (MPa) and coefficients of variation are presented.*

		Side pressure		
		0.5 (MPa)	**1.0 (MPa)**	**1.5 (MPa)**
growth ring angle	0°	34.19 (9.0)	36.89 (17.3)	39.36 (10.2)
	22°	21.18 (7.8)	20.04 (8.0)	18.55 (20.5)
	45°	9.14 (8.2)	7.44 (4.8)	7.11 (11.9)

*coefficient of variation (%) is given in parentheses.

Niemz (1993) reported a variability of the density between 0.30-0.64 g.cm^{-3} for spruce wood and a uniaxial compression strength of 40 MPa in the longitudinal direction.

Our results show that the axial component of the triaxial compression strength in the longitudinal direction is little below 40 MPa, but the density is at the lower bound of the range detected by Niemz. Therefore this deviation in the triaxial compression strength is not remarkable. Hence, increasing side pressures resulted in slightly increasing axial component of the triaxial strength in the longitudinal orientation. The mean values were 34.19 MPa at 0.5 MPa, 36.89 MPa at 1.0 MPa, and 39.36 MPa at 1.5 MPa side pressure.

However, the side pressure plays a more important role in the stiffness. The slope of the axial stress-strain diagrams show that a higher side pressure indicates a larger slope of the axial stress-strain curve, particularly in the longitudinally oriented specimens.

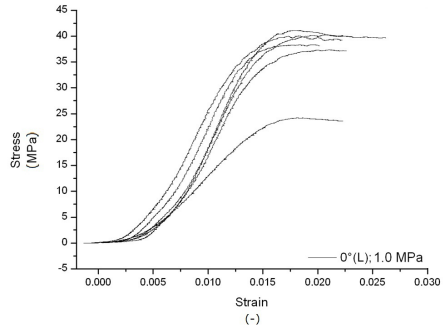

Fig. 5: Axial stress-strain curves for a test series in the longitudinal direction at 1.0 MPa side pressure.

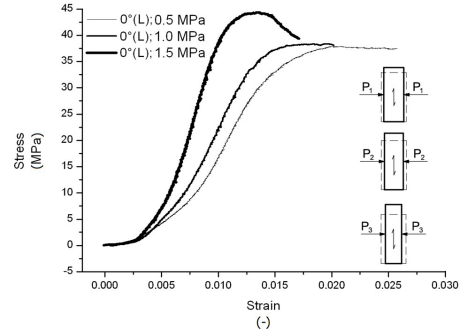

Fig. 6: Axial stress-strain curves for the longitudinal oriented specimens in case of 0.5, 1.0 and 1.5 MPa side pressure. Sketches show the influence of the side pressure.

Fig. 6 demonstrates the axial stress-strain relationship in the longitudinally oriented specimens for three different side pressures. The additional sketches represent the influence of

the side pressure on the strain of the sample. It is visible that the side pressure has a stiffening role in the longitudinally oriented samples. It should be noted that the slope of the stress-strain curve is not equal to the modulus of elasticity (MOE) because the complex stress states resulted in the extended Hooke`s law for anisotropic materials.

The mean values in the 22° orientation were 21.18 MPa at 0.5 MPa, 20.04 MPa at 1.0 MPa, and 18.55 MPa at 1.5 MPa side pressure. The mean values at 45° orientation were 9.14 MPa at 0.5 MPa, 7.44 MPa at 1.0 MPa, and 7.11 MPa at 1.5 MPa side pressure.

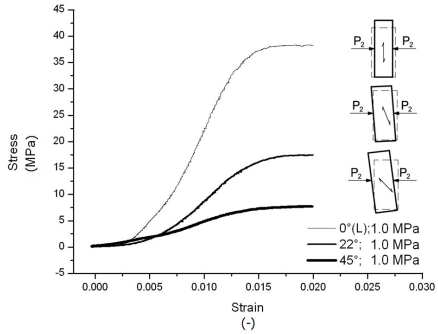

Fig. 7: Axial stress-strain curves of the samples with longitudinal (0°), 22° and 45° grain orientation under 1.0 MPa side pressure. Sketches show the shear effect of the side pressure depending on the orientation.

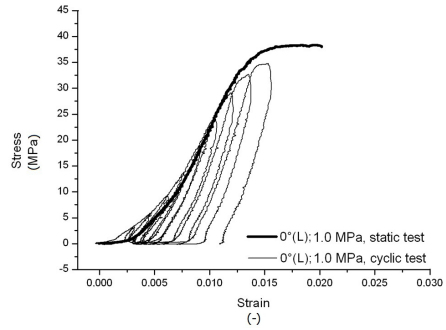

Fig. 8: Axial stress-strain diagrams of the static and the cyclic tests. The grain orientation was longitudinal and the side pressure was 1.0 MPa. The envelope of the cyclic diagram follows the static axial stress-strain diagram.

It should be mentioned that shear effects arose in the cross grained samples and it is hard to decide if the side pressure or the orientation is more important. The side pressure increases the stiffness in the longitudinal orientation but the shear effect due to the cross grain orientation can be significant. Similar to the uniaxial behavior, the axial strength decreased with increasing grain angle. Fig. 7 contains the stress-strain curves at the same side pressure and various grain orientations. The additional sketches represent the influence of the side pressure on strain only. Strain is significant in the cross grain direction. Therefore the shape will change.

The results of the cyclic tests (Fig. 8) show that the mechanical behavior is similar to that of the static tests. The slope of the linear part of the axial stress-strain diagram of each cycle is similar to that of the static curve. Thus, the Hookean behavior can be assumed for the cyclic multiaxial compression.

CONCLUSIONS

Triaxial compression tests confirmed that the triaxial servo-hydraulic testing machine is able to create multiaxial stress and deformation states on cylindrical wood specimens and the mechanical behavior of wood can be investigated. Although friction between steel plates and wood surfaces plays an important role, the side pressure is frictionless. Therefore, the use of oil pressure as side pressure is an advantage in comparison to other testing techniques on prismatic specimens. However, due to the complicated strain measurement, the determination of the real strain state and the measuring the elastic parameters is difficult. Another drawback is that the ring angle dependency cannot be measured due to the rotational symmetry of the specimen. Up

to now, the triaxial compression strength values were unavailable in the literature. Therefore the results are helpful in the investigation of the fracture characteristics of wood. In the future, the influence of side pressure can be an interesting topic to investigate the multiaxial compressive behavior of wood.

ACKNOWLEDGMENTS

This research was supported by the European Union and co-financed by the European Social Found in frame if the project "Talentum - Development of the complex condition framework for nursing talented students at the University of West Hungary", project ID: TÁMOP 4.2.2.B-10/1-2010-0018. Moreover, the first author is grateful to the Austrian Agency for International Mobility and Cooperation in Education, Science and Research (ÖAD) for the possibility of the student exchange.

REFERENCES

1. Ashkenazi, E.K., Lavrov, A.V., Myľnikova, O.S., Popov, V.D., 1973: Experimental investigation of the strength of anisotropic materials in biaxial and triaxial compression. Mechanics of Composite Materials 9(6): 879-884.
2. Bongers, J.P.W., Rutten, H.S., 1998: Concrete in multiaxial compression – a multilevel analysis. Heron 43(3): 159-180.
3. Eberhardsteiner, J., 2002: Mechanisches Verhalten von Fichtenholz – Experimentelle Bestimmung der biaxialen Festigkeitseigenschaften. Habilitation thesis. Springer-Verlag, Wien-New York, 174 pp.
4. Elkadi, A.S., van Mier, J.G.M., 2006: Experimental investigation of size effect in concrete fracture under multiaxial compression. International Journal of Fracture 140(1-4): 55-71.
5. Fleischmann, M., Krenn, H., Eberhardsteiner, J., Schickhofer, G., 2007: Experimental and numerical investigation of timber structures for the validation of an orthotropic plasticity model. (Numerische Berechnung von Holzkonstruktionen unter Verwendung eines orthotropen elasto-plastischen Werkstoffmodells). Holz als Roh- und Werkstoff 65(4): 301-313. (in German).
6. Forest Products Laboratory, 2000: Wood handbook – Wood as an engineering material. University Press of the Pacific, Honolulu, Hawaii.
7. Garab, J., Keunecke, D., Hering, S., Szalai, J., Niemz, P., 2010: Measurement of standard and off-axis elastic moduli and Poisson`s ratios of spruce and yew wood in the transverse plane. Wood Science and Technology 44(3): 451-464.
8. Garab, J., Szalai, J., 2010: Comparison of anisotropic strength criteria in the biaxial stress state. Drewno (Wood) 53(1): 51-66.
9. Gindl, W., Teischinger, A., 2002: Axial compression strength of Norway spruce related to structural variability and lignin content. Composites: Part A 33: 1623-1628.
10. Keunecke, D., Hering, S., Niemz, P., 2008: Three-dimensional elastic behaviour of common yew and Norway spruce. Wood Science and Technology 42(8): 633-647.
11. Kollmann, F., 1951: Technologie des Holzes und der Holzwerkstoffe. Band 1: Anatomie und Pathologie. Chemie, Physik, Elastizität und Festigkeit. Springer-Verlag, Berlin, Heidelberg, 1048 pp.

12. Mackenzie-Helnwein, P., Eberhardsteiner, J., Mang, H.A., 2005: Rate-independent mechanical behavior of biaxially stressed wood: Experimental observations and constitutive modeling as an orthotropic two-surface elasto-plastic material. Holzforschung 59(3): 311-321.
13. Neuhaus, F.H., 1981: Elastizitätszahlen von Fichtenholz in Abhängigkeit von der Holzfeuchtigkeit. Mitteilung Nr. 81-8, Inst. für konstruktiven Ingenieurbau. Dissertation Ruhr-University Bochum, Germany.
14. Niemz, P., 1993: Physik des Holzes und der Holzwerkstoffe. DRW, Leinfelden-Echterdingen, 243 pp.
15. Reiterer, A., Stanzl-Tschegg, S.E., 2001: Compressive behaviour of softwood under uniaxial loading at different orientations to the grain. Mechanics of Materials 33(12): 705- 715.
16. Saliklis, E.P., Cramer, S.M., Hermanson, J.C., 1998: Measuring the triaxial load-deformation response of orthotropic materials subjected to large and small strain regimes. Journal of testing and evaluation 26(5): 444-454.
17. Sasaki, Y., Yamasaki, M., 2002: Fatigue strength of wood under pulsating tension-torsion combined loading. Wood and Fiber Science 34(4): 508-515.
18. Sasaki, Y., Yamasaki, M., 2004: Effect of pulsating tension-torsion combined loading on fatigue behavior in wood. Holzforschung 58(6): 666-672.
19. Sasaki, Y., Yamasaki, M., Akita, F., 2007: Fatigue behavior in wood under pulsating compression-torsion-combined-loading. Wood and Fiber Science 39(2): 336-344.
20. Sasaki, Y., Yamasaki, M., Sugimoto, T., 2005: Fatigue damage in wood under pulsating multiaxial-combined loading. Wood and Fiber Science 37(2): 232-241.
21. Seweryn, A., Romanovych, M., 2007: Strength criteria for wood under the conditions of complexed stress state. Materials Science 43(3): 343-350.
22. Sfer, D., Carol, I., Gettu, R., Etse, G., 2002: Study of the behavior of concrete under triaxial compression. Journal of Engineering Mechanics 128(2): 156-163.
23. Szalai, J., 1998: Design values of acacia and spruce (*Robinia pseudoacacia* and *Picea excelsa*). Drevársky Výskum 43(3-4): 39-51.
24. Yamasaki, M., Sasaki, Y., 2003: Elastic properties of wood with rectangular cross section under combined static axial force and torque. Journal of Materials Science 38(3): 603-612.
25. Yamasaki, M., Sasaki, Y., 2004: Yield behavior of wood under combined static axial force and torque. Experimental Mechanics 44(3): 221-227.

József Garab
University of West Hungary
Institute for Applied Mechanics and Structures
Bajcsy Zs. Str. 4
9400 Sopron
Hungary
Phone: +36 99 518 254
Corresponding author: garabj@fmk.nyme.hu

Roland Reihsner, Josef Eberhardsteiner
Vienna University of Technology
Institute for Mechanics of Materials and Structures
Karlsplatz 13/202
1040 Vienna
Austria